EFFICIENT AND DETAILED MODEL OF THE LOCAL Ca^{2+} RELEASE UNIT IN THE VENTRICULAR CARDIAC MYOCYTE

THOMAS SCHENDEL
thomas.schendel@web.de

MARTIN FALCKE
martin.falcke@mdc-berlin.de

Max Delbrück Centre of Moleculare Medicine, Robert-Rössle-Str. 10, Berlin, Germany, 13092

We present here an efficient but detailed approach to modelling Ca^{2+}-induced Ca^{2+} release in the diadic cleft of cardiac ventricular myocytes. In this framework we developed a spatial resolved Ca^{2+} release unit (CaRU), consisting of the junctional sarcoplasmic reticulum and the diadic cleft, with a well defined channel placement. By taking advantage of time scale seperation, the model could be finally reduced to only one ordinary differential equation for describing Ca^{2+} fluxes and diffusion. Additionally the channel gating is described in a stochastic way. The resulting model is able to reproduce experimental findings like the gradedness of SR release, the voltage dependence of ECC gain and typical spark life time. Due to the numerical efficience of the model, it is suitable to use for whole cell simulations. The approach we want to use extend the developed CaRU to such a whole cell model is already outlined in this work.

Keywords: excitation-contraction coupling; calcium dynamics; modelling.

1. Introduction

The key step of excitation-contraction coupling (ECC) in cardiac myocytes, namely the Ca^{2+}-induced Ca^{2+} release(CICR) is a local phenomen, which takes place in very small subcompartments, the so called diadic clefts. The diadic cleft is the space between the membrane of the T-tubules on the one side and the junctional sarcoplasmic reticulum (JSR) on the other side. Membrane depolarisation leads to an activation of the L-type Ca^{2+}-channels (LCCs) in the membrane of the T-tubules, which causes a Ca^{2+}-influx into the diadic cleft. This Ca^{2+} activates the ryanodine receptors (RyRs) at the sarcoplasmic reticulum (SR), which release Ca^{2+} from the SR. That causes a large concentration rise in the diadic cleft and a partial depletion of the JSR. The small geometric properties of the diadic cleft provides the strong coupling between membrane depolarisation and Ca^{2+}-release.

The Ca^{2+} dynamics in the whole myocyte is modulated by further mechanisms. The main points are here the removal of Ca^{2+} from the myoplasm into the extracellular space via the Na^{+}-Ca^{2+}-exchanger or the Ca^{2+}-pumps, the reloading of the sarcoplasmic reticulum (SR) via the SERCA pumps and finally the Ca^{2+} buffers inside the cell.

Modelling the Ca dynamics in the whole ventricular myocyte is a challenging task due to the different time and length scales of the dynamics. On the one side the local mechanism of CICR in the diadic clefts (the volume of each cleft is in the range of 10^{-18}l), on the other side the global dynamics (implementing the different compartments, fluxes between this compartments and Ca^{2+}-buffers) has to be described. Finally, the diadic clefts (5,000-20,000 per cell [3, 4, 18] has to be included into the global model. Due to this (numerically) sophisticated task, former whole cell models have only simple models of the diadic cleft, which sometimes neglect the stochastic nature of the channel gating of LCCs or RyRs [9, 23] or treat the diadic cleft as one compartment with a uniform Ca^{2+} concentration and do not consider any spatial detail [9, 14, 23]. One exception is reported in Ref. [6], where the diadic cleft was divided into 4 different spatial parts. But this model is computionally expensive.

Nevertheless, there are also very detailed models of only the diadic cleft. These models are usually spatially resolved and stochastic [11, 18] and some even take explicitly the protein structure into account [18]. Nevertheless, these very detailed models lack of any global dynamics and they are computationally too demanding to be used as a CaRU in a global model.

The aim of this paper is to close the gap between a detailed, but numerical expensive description of the diadic cleft on the one side and numerically effecient whole cell models with a simple description of the local Ca^{2+} release unit (CaRU) on the other side. Therefore we want to present a detailed model of the local CaRU that is numerically efficient enough to use it for whole cell models. In our model the diadic cleft is spatially extended, with a defined channel placement. The channel gating is modelled in a stochastic manner. We also take into account the Ca^{2+} dynamics in the JSR.

Our model is able to reproduce basic experimental observations like gradedness (different amount of Ca^{2+} influx will trigger a different Ca^{2+} release from the SR), decreasing gain (defined by the ratio of Ca^{2+} release from SR to Ca^{2+} influx through LCCs) by increasing the membrane voltage and typical spark life time. It is therefore suitable to be used as a local CaRU in whole cell simulations. The description of our model will already gives some insight into how we want to extent the model to simulate the whole ventricular myocyte in future.

2. Model Description

The model of the local CaRU consists of three compartments, the diadic cleft, JSR and the cytosol bulk (see Fig. 1A). The RyRs at the JSR are colocalized to the LCC in the membrane of the T-tubules. We assumed the diadic cleft to be a cylinder with a height of 15 nm and a radius of 100 nm [17]. Because of the comparably small height, we effectively reduced the problem to a two-dimensional one by neglecting gradients orthogonal to the membranes. For a mathematical description of the CaRU, we had to deal with three different dynamics: the dynamics of the channel

states (of the LCCs and RyRs), the Ca^{2+} distribution in the diadic cleft and finally the Ca^{2+} dynamics in the JSR.

2.1. *Channel Placement and Gating*

We use 16 RyRs and 4 LCCs. The channel placement is seen in Fig. 1B. 4 RyRs are always close to one LCC, which reflects the experimental observation that the opening of one LCC can trigger the opening of 4-6 RyRs [20].

For the LCC we used the kinetic scheme from [9], which is a lumped state model. It consists of 3 states, open, closed and inactivated (Fig. 2A). Inactivation is in this scheme Ca^{2+} dependent. The rates have the following form [9]:

$$k_{CO} = \frac{e^{\frac{V-V_L}{dV_L}}}{t_L\left(e^{\frac{V-V_L}{dV_L}}+1\right)}$$

$$k_{OC} = \frac{\phi_L}{t_L}$$

$$k_{CI} = c_{di}\frac{e^{\frac{V-V_L}{dV_L}}+a}{K_L\tau_L\left(e^{\frac{V-V_L}{dV_L}}+1\right)}$$

$$k_{IC} = b\frac{e^{\frac{V-V_L}{dV_L}}+a}{\tau_L\left(e^{\frac{V-V_L}{dV_L}}+1\right)}$$

V...membrane voltage, c_{di}...Ca^{2+} concentration in the diadic cleft

For the RyRs we used a scheme developed in Ref. [2] (Fig. 2B). It consist of four states (rest, open and two inactivated states). The step to inactivation is Ca^{2+} dependent and the opening rate of the channel is a nonlinear function of Ca^{2+}.

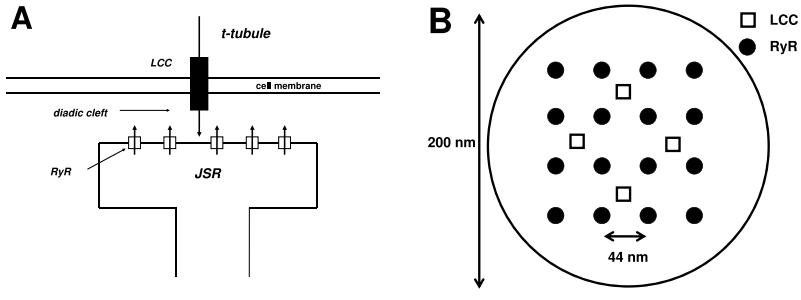

Fig. 1: (A) Scheme of the local CaRU, consisting of the diadic cleft and the JSR. RyRs and LCCs are colocalized. (B) The channel placement of 16 RyRs and 4 LCCs. Close to each LCC are 4 RyRs.

We decided to model the channel gating in a stochastic manner due to the experimental fact that a Ca^{2+} release event (Ca^{2+} spark) is built up by 1-7 open RyRs [21]. More details about the specific numerical treatment is provided in subsection 2D.

2.2. *Diffusion Profile in the Diadic Cleft*

Inside the diadic cleft we take into account the Ca^{2+} fluxes from LCCs and RyRs and Ca^{2+} diffusion ($c_{di}(\vec{r})$ denotes the Ca^{2+} concentration at the point $\vec{r}$ in the diadic cleft):

$$\frac{dc_{di}(\vec{r})}{dt} = \sum_i J^i_{LCC}(\vec{r_i}) + \sum_j J^j_{RyR}(\vec{r_j}) + D\Delta c_{di}(\vec{r}) \tag{1}$$

Because the typical diffusion time Δt for R=100 (radius of diadic cleft) nm is about $R = \sqrt{D\Delta t} \rightarrow \Delta t = 100\mu s$, which is much smaller than the typical time for the channel gating (usually in the range of ms), we can assume quasistationarity (see also [8]):

$$\frac{dc_{di}(\vec{r})}{dt} \approx 0 = \sum_i J^i_{LCC}(\vec{r_i}) + \sum_j J^j_{RyR}(\vec{r_j}) + D\Delta c_{di}(\vec{r}) \tag{2}$$

$$J^i_{LCC} = J_L \delta V \frac{c_{ext} e^{-\delta V} - c^i_{di}}{1 - e^{-\delta V}} \tag{3}$$

$$J^i_{RyR} = g(c^i_{JSR} - c^i_{di}) \tag{4}$$

$$c_{di}(r = R) = c_{bulk} \tag{5}$$

c_{JSR} denotes the Ca^{2+} concentration in the JSR, c_{ext} denotes the external Ca^{2+} concentration (set constant to $1000\mu M$). To simplify the following consideration, we will assume that c_{bulk} (Ca^{2+} concentration at the border of the diadic cleft) is constant and we will come back to this point at the end of this section. To calculate

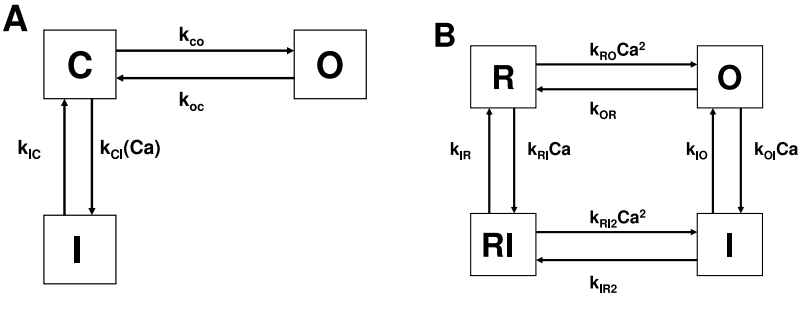

Fig. 2: Kinetic schemes for LCCs and RyRs. O denotes the open, C the closed, I the inactivated and R the resting state. (A) Kinetic scheme of the LCC from [9]. This scheme is a simplification of a more complex model. (B) Kinetic scheme from [2]. Activation is a nonlinear function of Ca^{2+}, Inactivation is Ca^{2+} dependent.

now the Ca^{2+} diffusion profile in the diadic cleft, we have to take the feedback of the concentration to the current into account: an opening of one channel will cause a flux which will lead to a Ca^{2+} concentration profile — which also affects the flux through this channel (as seen in Eq.(3)and (4)). In order to solve this problem, we obtained first an analytical solution for a simpler problem: one channel located in the middle of a circle with a radius r_c of $r_c = 6nm$ (typical radius of RyR) (we want to mention that the used fluxes and permeabilities are already scaled by the height h of the diadic cleft ($J = J_{real}/h$) in order to adjust to the two-dimensional problem):

$$\begin{aligned} -D\Delta c &= \tilde{g}(c_{JSR} - c)\ ;\ r \le r_c \\ -D\Delta c &= 0\ ;\ r > r_c \end{aligned} \tag{6}$$

and for the boundary condition

$$c(R) = c_{bulk} \tag{7}$$

The solution reads($k = \sqrt{\frac{\tilde{g}}{D}}$):

$$c(r) = c_{JSR} - \frac{c_{JSR} - c_{bulk}}{I_1(k\,r_c)\,ln\left(\frac{R}{r_c}\right)k\,r_c + I_0(k\,r_c)} I_0(k\,r)\,;\ r \le r_c \tag{8}$$

$I_0(kr)$ denotes the modified Bessel function of *0th* order. With this result one can calculate the mean Ca^{2+} concentration $\bar{c}$ at the channel and that allows to obtain the flux J through the channel. We now replaced the spatially extended channel by a δ-source with the same flux J. In general we obtain for the source coordinate $r = r_i$:

$$\begin{aligned} c(r) - c_{bulk} &= \frac{J}{\pi D}\sum_{k=0}^{\infty}\frac{B_0\left(x_{0,k}\frac{r_i}{R}\right)B_0\left(x_{0,k}\frac{r}{R}\right)}{x_{0,k}^2 J_1^2(x_{0,k})} \\ &+ \frac{2J}{\pi D}\sum_{n=1}^{\infty}\sum_{k=0}^{\infty}\frac{B_n\left(x_{n,k}\frac{r_i}{R}\right)B_n\left(x_{n,k}\frac{r}{R}\right)cos(n\varphi)}{x_{n,k}^2 J_{n+1}^2(x_{n,k})} \\ &= J\kappa(r_i, r) \end{aligned} \tag{9}$$

B_n denotes the Bessel function of nth order. $x(n,k)$ are the kth roots of the besssel function of nth order.
For comparison with Eq.(8) we chose $r_i = 0$. To circumvent the problem of the divergent δ-function at $r = 0$ we had to calculate the distance Δr, which satiesfies $c(\Delta r) = \bar{c}$ for $r_i = 0$. With this result we were able to calculate approximately the currents for arbitrarily chosen r_i:

1. Calculate the angle $\Delta\varphi = \arccos\left(1 - (\Delta r)^2/2r_i^2\right)$ where the mean calcium concentration of the channel is measured ($\bar{c} \approx c(r_i, \Delta\varphi)$)

2. Calculate $\bar{c}$ for a given flux J. Define $\kappa_i := \kappa(\vec{r_i}, \vec{r_i} + \Delta\vec{r_i})$. κ_i can be determined

by using Eq.(9): $\overline{c} = c_{bulk} + \kappa_i J$.

3. $J = g(c_{JSR} - \overline{c}) = g(c_{JSR} - c_{bulk} - \kappa_i J)$ (in case of a RyR) $\rightarrow J = \frac{g(c_{JSR} - c_{bulk})}{1 + \kappa_i g} \rightarrow$ $\overline{c} = c_{bulk} + (\kappa_i g(c_{JSR} - c_{bulk}))\,/\,(1 + \kappa_i g)$

The only approximation here is the use of the value of $|\Delta r|$ calculated with a channel in the centre of the cleft. If more than one channel is open, their produced Ca^{2+} concentration will affect each other. This situation ends up to a system of linear equations. For details, see Appendix 5.1.

2.3. *Ca^{2+} Dynamics in the JSR*

We assume that the JSR has a spatially uniform Ca^{2+} concentration. This Ca^{2+} concentration is affected by the outward flux J_{RyR} through the RyR and the refill flux from the network sarcoplasmic reticulum (NSR). We set the timescale for refilling to 30 ms [1]. Moreover, the Ca^{2+} buffer Calsequestrin was considered and for simplicity we chose the fast buffer approximation. We obtained:

$$\frac{dc_{JSR}}{dt} = \beta_{JSR}\left(-\frac{1}{V_{JSR}}\sum_j J^j_{RyR} + \frac{c_{NSR} - c_{JSR}}{\tau_{refill}}\right) \tag{10}$$

$$\beta_{JSR} = \left(1 + \frac{nK_c B_{CSQN}}{(K_c + c_{JSR})^2}\right)^{-1} \tag{11}$$

n...number of Ca^{2+}-binding sites of Calsequestrin, B_{CSQN}...concentration of Calsequestrin, K_C...dissociation constant of Calsequestrin (chosen from [14])
During all simulations, we keep the Ca^{2+} concentration in the NSR c_{NSR} constant ($c_{NSR} = 700\mu M$). To speed up simulations, we linearized β_{JSR} for each time step Δt around the actual $\widetilde{c}_{JSR}$, and obtained the following analytic expression:

$$c_{JSR} = \frac{\sqrt{-D}}{2a}\tanh\left(\operatorname{artanh}\left(\frac{2a\widetilde{c}_{JSR} + b}{\sqrt{-D}}\right) - \frac{\sqrt{-D}\Delta t}{2}\right) - \frac{b}{2a} \tag{12}$$

where a, b, c and D are defined by:

$$\frac{dc_{JSR}}{dt} = ac^2_{JSR} + bc_{JSR} + c$$

$$D = 4ac - b^2$$

2.4. *Matching the Dynamics Together*

On the one side we used a deterministic description of diffusion and the amount of flux through the open channels and on the other side we used a stochastic approach for the channel gating. Such a "mixed approach" was justified in [8]. In case of comparably quick channel state transitions, the Ca^{2+} concentration in the JSR (and therefore the Ca^{2+} profile in the diadic cleft) remains nearly unchanged between transitions and we could use the efficient Gillespie algorithm [5]. In case of slower channel transition the Ca^{2+} concentration changes in the JSR (and therefore the

Ca^{2+} concentration changes in the diadic cleft) are not negligible and we have to use a hybrid algorithm for the stochastic stimulation described in [15]. Our algoritm works as follows:

Assume that N channel transitions are possible with the associated propensities (rates) $\alpha_1 ... \alpha_N$. Following the Gillespie algorithm (assuming that the propensities are not changing) the time step τ until the next channel transition takes place is defined by:

$$\sum_{i}^{N} \alpha_i \tau = \ln 1/r_1 \tag{13}$$

r_1 is a uniform random number in the interval [0,1]. If during this time τ the Ca^{2+} concentration in the JSR remains nearly constant, we can apply the Gillespie algorithm. Otherwise the Ca^{2+} concentration in the diadic cleft and therefore the propensities α_i are time dependent. In this case the time τ is defined by ([15]):

$$\int_{t}^{t+\tau} \sum_{i}^{N} \alpha_i(s) ds = \ln 1/r_1 \tag{14}$$

In the simulations we divided the integral into smaller time steps during which the concentration in the JSR remains nearly constant.

2.5. *Calculating the Ca^{2+} Concentration at the Boundary of the Diadic Cleft*

The bulk Ca^{2+} concentration is mainly influenced by the diadic cleft itself. We assumed one diadic cleft (modelled as a point source) in the middle of the cell (modelled as a cylinder with a radius R_m of $R_m = 11\mu m$ and a length L of $L = 140\mu m$). We take into account the pumping of Ca^{2+} from the myoplasma into the NSR via SERCA, the mobile Ca^{2+} buffer Calmodulin (denoted in the equations as M for the unbounded form), the immobile Ca^{2+} buffer Troponin (denoted in the equations as T) and a constant leak flux from the NSR (that maintains in equilibrium a resting Ca^{2+} concentration of $0.1\mu M$):

$$\begin{aligned}
\frac{\partial c}{\partial t} &= D_c \Delta c + J_{leak} - g_{SERCA} \frac{c^2}{K_m^2 + c^2} - k_+^M cM + k_-^M (B_M - M) \\
&\quad - k_+^T cT + k_-^T (B_T - T) \\
\frac{\partial M}{\partial t} &= D_M \Delta M - k_+^M cM + k_-^M (B_M - M) \\
\frac{\partial T}{\partial t} &= -k_+^T cT + k_-^T (B_T - T)
\end{aligned} \tag{15}$$

We want to solve this system of PDEs by using three component Green's functions. Therefore we had to linearize the system of Eq.(15) around $c_{rest} = 0.1\mu M$ and we

got:

$$\begin{aligned}
\frac{\partial \delta c}{\partial t} &= D_c \Delta \delta c - \rho_{SERCA} \delta c - k_+^M \delta c M_0 - k_+^M \delta M c_0 - k_+^T \delta c T_0 - k_+^T \delta T c_0 \\
\frac{\partial \delta M}{\partial t} &= D_M \Delta \delta M - k_+^M \delta c M_0 - k_+^M \delta M c_0 \\
\frac{\partial \delta T}{\partial t} &= -k_+^T \delta c T_0 - k_+^T \delta T c_0
\end{aligned} \tag{16}$$

The Green's functions can be seen in the Appendix 5.2. By simulations we obtained that the stationary solution is sufficient at the boundary of the cleft to calculate the bulk Ca^{2+} concentration. That is not really surprising, because of the used small length scales where the diffusion is dominant (typical diffusion time for R=100 nm is 100 μs calculated in 2.2). The stationary cytosolic concentration at the boundary of the celft c_{bulk} is again proportional to the total flux J out of the diadic cleft: $c_{bulk} - c_{rest} = \beta J$ (the way to calculate β is shown in the Appendix 5.2). c_{bulk} enters the current and concentration calculation according to Eq. 17 in Appendix 5.1.

3. Results

The local CaRU has for it's validation to reproduce general experimental results. One important property is gradedness, which means that a different Ca^{2+} influx through LCCs will trigger a different amount of Ca^{2+} release from the SR. In Fig. 3A the integrated Ca^{2+} fluxes (over 100ms) through RyRs and LCCs is depicted. It is seen that the model is able to exhibit gradedness. The maximum of Ca^{2+} release from SR is shifted by about 10mV with respect to the the maximum of Ca^{2+} entry through LCCs. This is due to the higher sensitivity of RyRs to higher single LCC currents (which occur after the Goldmann-Hodgkin-Katz equation (Eq.(3))

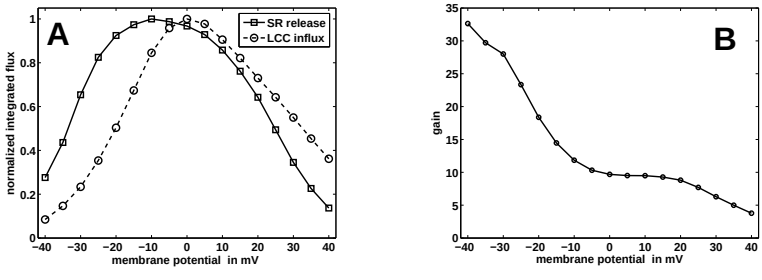

Fig. 3: A) Over 100 ms integrated Ca^{2+} fluxes through RyR and LCC as a function of membrane potential. The peak for Ca^{2+} release from SR is around 10 mV shifted from the peak of Ca^{2+} entry through LCC. (B) Gain defined as the ratio of Ca^{2+} release from SR to Ca^{2+} entry via LCC. It decreases for increasing membrane potential. Here are two figures side-by-side. (a) Figure caption for figure 2a. (b) Figure caption for figure 2b.

for smaller membrane potentials) and reproduces the experimental data [22]. If we now define the property gain as the ratio between the Ca^{2+} release from the SR to the Ca^{2+} entry from the LCC, we can plot it as a function of membrane potential. This curve is a decreasing function of membrane potential (Fig. 3B), which is in accordance with experiment [22].

We also studied the dependence of ECC for variable distances from the t-tubule to JSR. In Fig. 4A gain was plotted for three different heights. It is seen that the gain decreases for increasing height. Since gain is simply an indicator for the strength of the coupling between membrane depolarisation and Ca^{2+} release, ECC decreases with increasing height of the diadic cleft.

Finally, we studied the spark time distribution (Fig. 4B). We defined the time of a spark as the time between when the first RyR opens until all RyRs are closed. The mean spark life time was determined to $9.8ms$, which is in the range of experimental measurements ($11.6ms$ [21]).

4. Discussion

In this paper we have described a detailed model of the local CaRU that is numerically fast enough to be used for whole cell simulations. The model describes individual RyRs and LCCs as stochastic Markov chains, the concentration profiles inside the cleft, the interaction of channel currents resulting from them and the concentration dynamics in the JSR. Computational efficiency is achieved by a quasistatic approximation for the concentration profiles inside the cleft. The cleft model reproduces basic experimental findings like gain and gradedness, average spark life times and the dependence of gain on cleft height.

Former papers focusing on whole cell simulations often used only simple forms of the local CaRU, mostly without a spatially resolved diadic cleft. Hinch et al. [9] and Williams et al. [23] treat the diadic cleft only as a uniform single compartment, using deterministic models for LCC and RyR. In the work of Restrepo et al. [14]

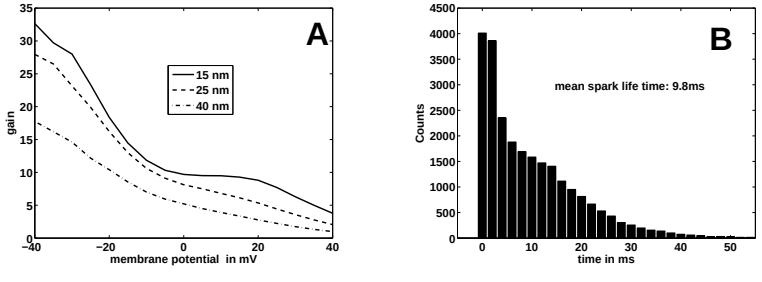

Fig. 4: (A) Gain for different heights of the diadic cleft: h=15, 25, 40 nm. The coupling decreases for increasing height. (B) Spark time distribution over an samplesize of 24261 sparks for V=0 mV and 15 nm height of the diadic cleft.. The mean spark life time was obtained to 9.8 ms.

are additionally several channels used which are treated in a stochastic way, but the diadic cleft was not modelled in a spatially resolved way. Greenstein et al. [6] considered some spatial structure and concentration gradients by introducing compartments for each of 4 pairs of one LCC and 5 RyRs, simulated each channel as Markov chain and concentrations dynamically with rate equations. Our approach is more flexible with respect to channel numbers, more detailed with respect to spatial structure and computationally more efficient, since integrate only the differential equation for c_{JSR} along with the Markov simulations.

There is also a wide class of papers dealing only to modell the diadic cleft. For example Tanskanen et al. [18], treat the diadic cleft not only spatially resolved, but also takes explicitly into account the protein structure in the diadic cleft and membrane buffers. The channel gating and the flux through open channels is treated stochastically. A similar approch was presented in Koh et al. [11]. Nevertheless this models are very time expensive and not suitable for whole cell simulations.

The introduced approach opens up new possibilities to study the influence of altering channel properties in the framework of the whole cell. Interesting phenomena in this background are for instance channel phosphorylation or cooperative RyR gating. Channel phoshorylation can be mediated by the cAMP/PKA pathway due to β-adrenergic stimulation. This leads to an increase of the flux through RyRs and LCCs [7, 10, 13]. Another example would be the effect of cooperating RyRs. The RyR are linked with their neighbours by a protein (FKBP), which couples the gating of the channels [12, 19].

5. Appendix

5.1. *Ca^{2+} Profile for more than One Open Channel and with Varying Bulk Concentration*

For solving the problem with N channels, it is necessary to introduce channel related concentrations c_i. $c_i(r)$ describes the part of the Ca^{2+} concentration at position r, that is produced by the ith channel. Furthermore, we introduce $\alpha_{i,j} = \frac{c_i(r_j)}{c_i(r_i)}$. For the Ca^{2+} bulk concentration, we have to determine the parameter β by $c_{bulk} - c_{rest} = \beta \sum_i J_i$. For an understandable derivation we just show only the case of open RyRs, an extension for LCCs is straight forward. In order to solve the problem, we obtained

following system of linear equations:

$$\begin{aligned}
\overline{c_1} &= \kappa_1 g \left(c_{JSR} - c_{bulk} - \overline{c_1} - \sum_{j\neq 1}^{N} \alpha_{j,1}\overline{c_j} \right) \\
\overline{c_2} &= \kappa_2 g \left(c_{JSR} - c_{bulk} - \overline{c_2} - \sum_{j\neq 2}^{N} \alpha_{j,2}\overline{c_j} \right) \\
&\dots \\
\overline{c_N} &= \kappa_N g \left(c_{JSR} - c_{bulk} - \overline{c_N} - \sum_{j\neq N}^{N} \alpha_{j,N}\overline{c_j} \right) \\
c_{bulk} - c_{rest} &= \beta \sum_{i}^{open} J_i
\end{aligned} \tag{17}$$

In the maximal case that all channels are open we end up with a 21x21 matrix, which can be solved numerically fast.

5.2. *Green's Function*

We assumed the myocyte as a cylinder with $r \in [0, R]$ and $z \in [-\frac{L}{2}, \frac{L}{2}]$. To solve the system of PDE (15), the Green's function $\tilde{G}$ must in general take the form:

$$\tilde{G} = \sum_{k,m=0}^{\infty} \sum_{n=0}^{\infty} \alpha_{k,m,n} B_0(x(k)\frac{r}{R}) B_0(x(k)\frac{r'}{R}) cos(m\pi\frac{z}{L}) cos(m\pi\frac{z'}{L}) cos(n(\varphi - \varphi')) \tag{18}$$

with the bessel function of the first kind, $0th$ order $B_0(r)$ which satiesfies the Helmholtz equation. The eigenvalues *x(k)* are determined by the boundary condition at R (the cell radius) of no fluxes:

$$\frac{\partial B_0(x(k)\frac{r}{R})}{\partial r}|_{r=R} = 0 \tag{19}$$

In the particular case of one δ-source located at $r' = 0$ and $z' = 0$ Eq.(18) simplifies to

$$\tilde{G} = \sum_{k,m=0}^{\infty} \tilde{\alpha}_{k,m} B_0(x(k)\frac{r}{R}) cos(2m\pi\frac{z}{L}) \tag{20}$$

After some steps with using Eq.(16) and the fact that we have only a single δ-channel at the centre of the cell we arrive at (for more details, see [16]):

$$\begin{pmatrix} \delta c \\ \delta M \\ \delta T \end{pmatrix}(t) = \sum_{k=0}^{\infty} \sum_{m=0}^{\infty} B_0(x(k)\frac{r}{R}) cos(2m\pi\frac{z}{L}) \begin{pmatrix} \chi_1^{(k,m)} \\ \chi_2^{(k,m)} \\ \chi_3^{(k,m)} \end{pmatrix} (\vec{r'} = \vec{0}, t) \tag{21}$$

The response functions $\vec{\chi}^{(k,m)}$ include the time integration over the time dependent channel flux J and includes the interaction with the buffers as well as the pumping to the SR:

$$\begin{pmatrix} \chi_1^{(k,m)} \\ \chi_2^{(k,m)} \\ \chi_3^{(k,m)} \end{pmatrix} = \sum_{i=0}^{3} \frac{1}{N_{k,m}} \int_0^t d\tau J(\tau) e^{-s_i(t-\tau)} \frac{adj(M_{km}(s_i))}{\partial |M_{km}|/\partial s|_{s=s_i}} \begin{pmatrix} 1 \\ 0 \\ 0 \end{pmatrix} \tag{22}$$

with the normalization factor N (for $k, m \neq 0$):

$$N_{k,m} = \int_0^R \int_0^{2\pi} \int_{-\frac{L}{2}}^{\frac{L}{2}} dr d\varphi dz r B_0(x(k)\frac{r}{R}) cos(2m\pi\frac{z}{L}) = \frac{\pi R^2 L}{2} \tag{23}$$

The s_i of the response function can be determined by $det(M_{km}) = 0$. M is given by:
$M_{km}=$

$$\begin{pmatrix} -D_c x(k)^2 - s - \rho_{SERCA} - k_+^M M_0 - k_+^T T_0 & -k_+^M c_0 & -k_+^T c_0 \\ -k_+^M M_0 & -D_M x(k)^2 - s - k_+^M c_0 & 0 \\ -k_+^T T_0 & 0 & -s - k_+^T c_0 \end{pmatrix}$$

5.3. *Parameters*

Table 1 RyR parameters LCC parameters

Parameter	Value	Parameter	Value
g	$10\mu m^3 s^{-1}$	J_L	$0.913\mu m^3 s^{-1}$
k_{RO}	$0.015\mu M^{-2} s^{-1}$	V_L	$-2mV$
k_{OR}	$60s^{-1}$	$\Delta V_L r$	$7mV$
k_{IO}	$5s^{-1}$	ϕ_L	6.667
k_{OI}	$0.5\mu M^{-1} s^{-1}$	t_L	$0.0033s$
k_{IR}	$5s^{-1}$	τ_L	$0.65s$
k_{RI}	$0.5\mu M^{-1} s^{-1}$	K_L	$0.22\mu M$
k_{IR2}	$60s^{-1}$	a	0.0625
k_{RI2}	$0.015\mu M^{-2} s^{-1}$	b	14

Table 2 Other parameters

Parameter	Value	Parameter	Value
c_{ext}	$1000\mu M$	k_M^+	$100\mu M^{-1} s^{-1}$
c_{NSR}	$700\mu M$	k_M^-	$38s^{-1}$
D_c	$100\mu m^2 s^{-1}$	k_T^+	$40\mu M^{-1} s^{-1}$
B_{CSQN}	$400\mu M$	k_T^-	$40s^{-1}$
K_c	$600\mu M$	B_M	$24\mu M$
τ_{refill}	$7.5ms$	B_T	$70\mu M$
ρ_{SERCA}	$390s^{-1}$		

References

[1] Brochet, D.X.P., Yang, D.M., Di Maio, A., Lederer, J., Franzini-Armstrong, C., Cheng, H.P. Ca^{2+} blinks: rapid nanoscopic store calcium signaling. *Proc. Natl. Acad. Sci.USA.*, 102:3099–3104, 2005.

[2] Cheng, H., Fill, M., Valdivia, H., Lederer, W.J., Models of Ca^{2+} release channel adaption. *Science*, 267:2009–2011, 1995.

[3] Chen-Izu, Y., McCulle, S.L., Ward, C.W., Soeller, C., Allen, B.M., Rabang, C., Cannell, M.B., Balke, C.W., Izu, L. Three-Dimensional Distribution of Ryanodine Receptor Clusters in Cardiac Myocytes. *Biophy. J.*, 91:1–13, 2006.

[4] Cleeman, L., Wang, W., Morad, M. Two-dimensional confocal images of organization, density, and gating of focal Ca^{2+} release sites in rat cardiac myocytes. *Proc. Natl. Acad. Sci.USA.*, 95:10984–10989, 1998.

[5] Gillespie, D.T., Exact stochastic simulation of coupled chemical reactions. *J. Phys. Chem.*, 81: 2340–2361, 1977.

[6] Greenstein, J.L., Winslow, R.L., An integrative model of the cardiac ventricular myocyte incorporating local control of Ca^{2+} release. *Biophy. J.*, 83:2918–2945, 2002.

[7] Hain, J., Onoue, H., Mayrleitner, M., Fleischer, S., Schindler, H., Phosphorylation modulates the function of the calcium release channel of sarcoplasmic reticulum from cardiac muscle. *J.Biol.Chem.*, 270:2074–2081, 1995.

[8] Hake, J., Lines, G.T., Stochastic binding of Ca^{2+} ions in the dyadic cleft; continious vs. Random Walk description of diffusion. *Biophys. J.*, 94:4184–4201, 2008.

[9] Hinch, R., Greenstein, J.L., Tanskanen, A.J., Xu, L., Winslow, R.L., A simplified local control model of calcium-induced calcium release in cardiac ventricular myocytes. *Biophy. J.*, 85:3723–3736, 2004.

[10] Kamp, T.J., Hell, J.W., Regulation of cardiac L-type calcium channels by protein kinase A and protein kinase C. *Circ. Res.*, 87:1095–1102, 2000.

[11] Koh, X., Srinivasan, B., Ching, H.S., Levchenko, A., A 3D Monte Carlo analysis of the role of dyadic space geometry in spark generation. *Biophys. J.*, 90:1999–2014, 2006.

[12] Marx, S.O., Gaburjakova, J., Gaburjakova, M., Hendrikson, C., Ondrias, K., Marks, A.R., Coupled gating between cardiac Ca^{2+} release channels (ryanodine receptors). *Circ.Res.*, 88:1151–1158, 2001.

[13] Reiken, S., Garbujakova, M., Guatimosin, S., Gomez, A.M., D'Armiento, J., Burkhoff, D., Wang, J., Vassort, G., Lederer, W.J., Marks, A.R., Protein kinase A phosphorylation of the cardiac calcium release channel (ryanodine receptor) in normal and failing hearts. Role of phosphotases and response to isoprotenerol. *J.Biol.Chem.*, 278:444–453, 2003.

[14] Restrepo, J.G., Weiss, J.N., Karma, A., Calsequestrin-Mediated Mechanism for Cellular Calcium Transient Alternans. *Biophy. J.*, 95:3767–3789, 2008.

[15] Rüdiger, S., Shuai, J.W., Huisinga, W., Nagaiah, C., Warnecke, G., Parker, I., Falcke, M., Hybrid stochastic and deterministic simulations of calcium blips. *Biophy. J.*, 93:1847–1857, 2007.

[16] Skupin, A., Falcke, M., The role of IP_3R clustering in Ca^{2+} signaling. *Genome Informatics*, 20:15–24, 2008.

[17] Soeller, C., Cannel, M.B., Numerical simulation of local calcium movements during L-type calcium channel gating in the cardiac diad. *Biophy. J.*, 73:97–111, 1997.

[18] Tanskanen, A.J., Greenstein, J.L., Chen, A., Sun, S.X., Winslow, R.L., Protein geometry and placement in the cardiac dyad influence macroscopic properties of calcium-induced calcium release. *Biophy. J.*, 92:3379–3396, 2007.

[19] Wagenknecht, T., Badermacher, M., Grassucci, R., Berkowitz, J., Xin, H.B., Fleischer,

S., Locations of calmodulin and FK506-binding protein on the three-dimensional architecture of the sceletal muscle ryandine receptor. *J.Biol.Chem.*, 272:32463–32471, 1997.

[20] Wang, S.Q., Song, L.S., Lakkata, E.G., Cheng, H., Ca^{2+} signalling between single L-type Ca^{2+} channels and ryanodine receptors in heart cells. *Nature*, 410:592–596, 2001.

[21] Wang, S.Q., Stern, M.D., Rios, E., Cheng, H., The quantal nature of Ca^{2+} sparks and in situ operation of the ryanodine receptor array in cardiac cells. *Proc. Natl. Acad. Sci.USA.*, 101:3979–3984, 2003.

[22] Wier, W.G., Egan, T.M., Lopez-Lopez, J.R., Balke, C.W., Local control of excitation-contraction coupling in rat heart cells. *J.Physiol.*, 474:463–471, 1994.

[23] Williams, G.S.B., Huertas, A.H., Sobie, E.A., Jafri, M.S., Smith, G.D., A Probabilty density approach to modeling local control of calcium-induced calcium release in cardiac myocytes. *Biophy. J.*, 92:2311–2328, 2007.